Critical behavior of gravitating sphalerons

R. Steven Millward* and Eric W. Hirschmann†
Department of Physics and Astronomy, Brigham Young University, Provo, Utah 84604, USA
(Received 19 December 2002; published 10 July 2003)

We examine the gravitational collapse of sphaleron type configurations in the Einstein-Yang-Mills-Higgs theory. Working in spherical symmetry, we investigate the critical behavior in this model. We provide evidence that for various initial configurations, there can be three different critical transitions between possible end states with different critical solutions sitting on the threshold between these outcomes. In addition, we show that within the dispersive and black hole regimes there are new possible end states: namely, a stable, regular sphaleron and a stable, hairy black hole.

DOI: 10.1103/PhysRevD.68.024017 PACS number(s): 04.25.Dm

I. INTRODUCTION

Over the past two decades, substantial effort has been brought to bear on the study of the gravitating Yang-Mills fields. This research has resulted in the discovery of numerous solutions to the coupled Einstein-Yang-Mills(-Higgs and/or -dilaton) equations. These solutions include both black hole and regular or particlelike solutions. In addition to confirming the richness of these nonlinear systems, this work has also been helpful in clarifying the standing of the black hole uniqueness theorems and various ''no-hair'' ideas.

While many of these solutions have been found by solving the appropriate static equations, it was realized early on that understanding the stability of these solutions is important in order to ascribe relative significance to these solutions within the context of some of the no-hair conjectures. The primary means for evaluating stability have been linear perturbation analyses of various static solutions. As a result, many of these static, gravitating Yang-Mills(-scalar) configurations have been found to be unstable to small time-dependent perturbations.

That many of these solutions appear unstable in linear perturbation theory does not necessarily mean that such solutions are without significance. Indeed, it is now widely accepted within the context of gravitational critical phenomena that some of these solutions will have relevance as attractors in the critical collapse of gravitating fields at the threshold of black hole formation [1,2]. As an example, the Bartnik-McKinnon solutions of the spherically symmetric, static Einstein-Yang-Mills equations are a countably infinite family of regular solutions characterized by the integer number n of zero crossings of the gauge potential. These solutions are unstable in linear perturbation theory with the n^{th} member of the family having n unstable modes.[1] Thus, the $n=1$ member of this family has a single unstable mode and is a candidate for being a critical solution in the gravitational collapse of a pure Yang-Mills field. Indeed, this is exactly the result found in [4] where the full evolution equations for the model were solved. The $n=1$ Bartnik-McKinnon solution is the critical solution that sits on the threshold between the complete dispersal of the collapsing field and the formation of a finite size black hole (type I collapse). The value of the unstable mode for this solution then correctly predicts the scaling relation for the lifetime of near-critical solutions.

In addition to these regular solutions, the Einstein-Yang-Mills equations also admit another countably infinite family of solutions, but with a horizon. These black hole solutions have non-trivial hair outside their horizons and are again characterized by the number n_{BH} of zero crossings of the gauge potential. They too are unstable in linear perturbation theory with n_{BH} unstable modes from the gravitational sector. In agreement with expectations, it has been shown that the $n_{\text{BH}}=1$ solution is also a critical solution [5]. But this non-Abelian or colored black hole solution, rather than separating dispersion and black hole formation as does the $n=1$ Bartnik-McKinnon solution, sits on the threshold between two different kinds of dynamical collapse.

Given this behavior, it is natural to conjecture that other configurations of gravitating Yang-Mills fields should likewise exhibit critical phenomena. With that in mind, we consider here the nonlinear evolution of gravitating $SU(2)$ sphalerons in the Einstein-Yang-Mills-Higgs theory. We provide evidence that there can be three critical transitions in the initial data space. These include the now standard type I and type II transitions as well as the transition mentioned above between different kinds of dynamical collapse on which sits a colored or hairy black hole as the intermediate attractor. In the process of examining critical gravitational collapse within this system and the formation of such ''hairy'' black holes as attractors in the black hole regime, we have also confirmed the stability of two additional end states of collapse. One is a regular, gravitationally bound configuration of the Yang-Mills-Higgs field forming a stable ''sphaleron star.'' The second is a family of stable, hairy black holes different from those that serve as the critical solutions in the black hole regime. The existence of such stable solutions appears to have been first predicted by Maison [6].

The outline of the remainder of the paper is then as fol-

*Electronic address: rsm52@email.byu.edu
†Electronic address: ehirsch@kepler.byu.edu

[1]Strictly, this is true if only the radial, gravitational perturbations are excited. If additional components of the gauge potential are also perturbed (i.e., the sphaleron sector), the nth solution will have $2n$ unstable modes, the sphaleron sector contributing an additional n unstable modes to those from the gravitational sector [3].

lows. Section II summarizes the equations which constitute the full evolution problem and our numerical approach to their solution. Section III describes the numerical results, including results of our parameter space searches, the critical solutions and the nature of the stable solutions. Section IV offers some conclusions and thoughts for future directions.

II. THE MODEL

Our starting point in studying the gravitational collapse of configurations of the Yang-Mills-Higgs fields is the action

$$S=\int d^4x\sqrt{-g}\left[\frac{1}{16\pi G}R-\frac{1}{4g^2}F^a_{\mu\nu}F^{a\mu\nu}-\frac{1}{2}(D_\mu\Phi)^\dagger D^\mu\Phi-V(|\Phi|^2)\right] \quad (1)$$

where $F^a_{\mu\nu}$ is the Yang-Mills field strength tensor given by

$$F^a_{\mu\nu}=\partial_\mu A^a_\nu-\partial_\nu A^a_\mu+\epsilon^{abc}A^b_\mu A^c_\nu, \quad (2)$$

D_μ is the gauge covariant derivative whose action on the Higgs doublet Φ is

$$D_\mu\Phi=\nabla_\mu\Phi+A_\mu\Phi, \quad (3)$$

and the potential V is taken to be

$$V(|\Phi|^2)=\frac{\lambda}{4}(\Phi^\dagger\Phi-\eta^2)^2. \quad (4)$$

Varying the action with respect to the metric, the field strength and the Higgs field result in the Einstein equations and the curved space Yang-Mills and Higgs equations, respectively. These are

$$\frac{1}{8\pi G}G_{\mu\nu}=\frac{1}{g^2}\left[F^a_{\mu\lambda}F^{a\lambda}_\nu-\frac{1}{4}g_{\mu\nu}F^a_{\alpha\beta}F^{a\alpha\beta}\right]+(D_\mu\Phi)^\dagger D_\nu\Phi-\tfrac{1}{2}g_{\mu\nu}(D_\lambda\Phi)^\dagger D^\lambda\Phi-g_{\mu\nu}V(|\Phi|^2) \quad (5)$$

$$\nabla_\mu F^{a\mu\nu}+\epsilon^{abc}A^b_\mu F^{c\mu\nu}+\mathrm{tr}([\tau^b\partial_\mu\tau^a])F^{b\mu\nu}=\tfrac{1}{2}[(D^\nu\Phi)^\dagger\tau^a\Phi-\Phi^\dagger\tau^a D^\nu\Phi] \quad (6)$$

$$D^\mu D_\mu\Phi=\lambda\,\Phi(\Phi^\dagger\Phi-\eta^2). \quad (7)$$

With these general forms for the equations of motion, we make some simplifying assumptions. In particular, we will restrict ourselves to spherically symmetric gravitational collapse and work exclusively with an $SU(2)$ gauge group. We also make the assumption that the Higgs field lives in the fundamental representation of $SU(2)$. The corresponding flat space version of this theory includes the so-called sphaleron solutions [7]. We also set $g=1$.

Our intent is to solve the full set of nonlinear, evolution equations representing gravitational collapse. In order to do this numerically we must fix both the coordinate freedom and the gauge freedom in our model. There are, of course, numerous possibilities, but we will try to hew fairly closely to related work of others in the field. For the coordinate system, we will work in maximal, areal coordinates. If the general form of the spherically symmetric metric is written as

$$ds^2=(-\alpha^2+a^2\beta^2)dt^2+2a^2\beta dtdr+a^2dr^2+b^2r^2d\theta^2+b^2r^2\sin^2\theta d\phi^2 \quad (8)$$

where the metric components depend only on t and r, the choice of areal coordinates amounts to $b=1$ while choosing maximal time slices corresponds to the vanishing of the trace of the extrinsic curvature, $K=0$.

For the Yang-Mills field, the most general form for a spherically symmetric gauge potential is the Witten ansatz [8]:

$$A=u\,\tau_r dt+v\,\tau_r dr+[w\,\tau_\theta+(\tilde{w}-1)\tau_\phi]d\theta+[(1-\tilde{w})\tau_\theta+w\,\tau_\phi]\sin\theta d\phi \quad (9)$$

where τ_i $(i\in\{r,\theta,\phi\})$ are the spherical projection of the Pauli spin matrices and form an anti-Hermitian basis for the group $SU(2)$ satisfying $[\tau_i,\tau_j]=\epsilon_{ijk}\tau_k$. With this ansatz for the gauge potential there is some gauge freedom that allows us to simplify its form: namely, the potential is invariant under a transformation of the form $U=e^{\psi(t,r)\tau_r}$. We can fix

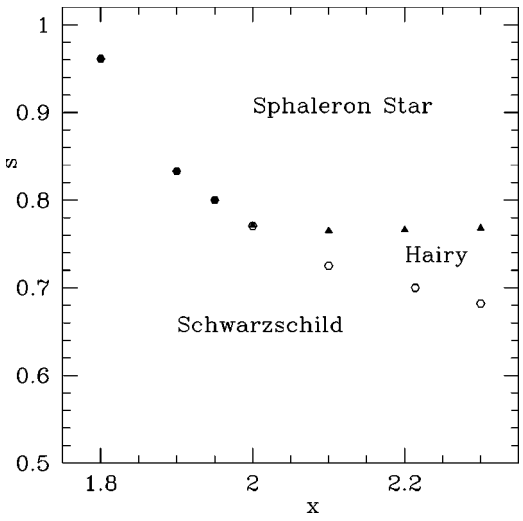

FIG. 1. This plot is of the initial data space and illustrates the end states of collapse as the width s and center x of the initial Yang-Mills field are varied. The Higgs field is in the "bland" configuration, i.e., $\delta=10$ and $A_H=0$. The filled hexagons give the boundary between the formation of the sphaleron star solutions and the Schwarzschild black holes. The filled triangles represent the boundary between the formation of the sphaleron stars and the hairy black holes. The open hexagons depict the hairy critical solutions on the boundary between the Schwarzschild and hairy black holes. Near these critical solutions, the type is depicted not only by the existence of the stable hair, but also by the transient hair either dispersing or falling down the horizon. Note the similarity between this and Fig. 4 of [5]. Each point depicted on the plot represents an evolution in which $|p-p^*|<10^{-5}$. For each evolution we used 10401 mesh points and a Courant factor of 0.5 along with $\eta=0.1$ and $\lambda=0.5$.

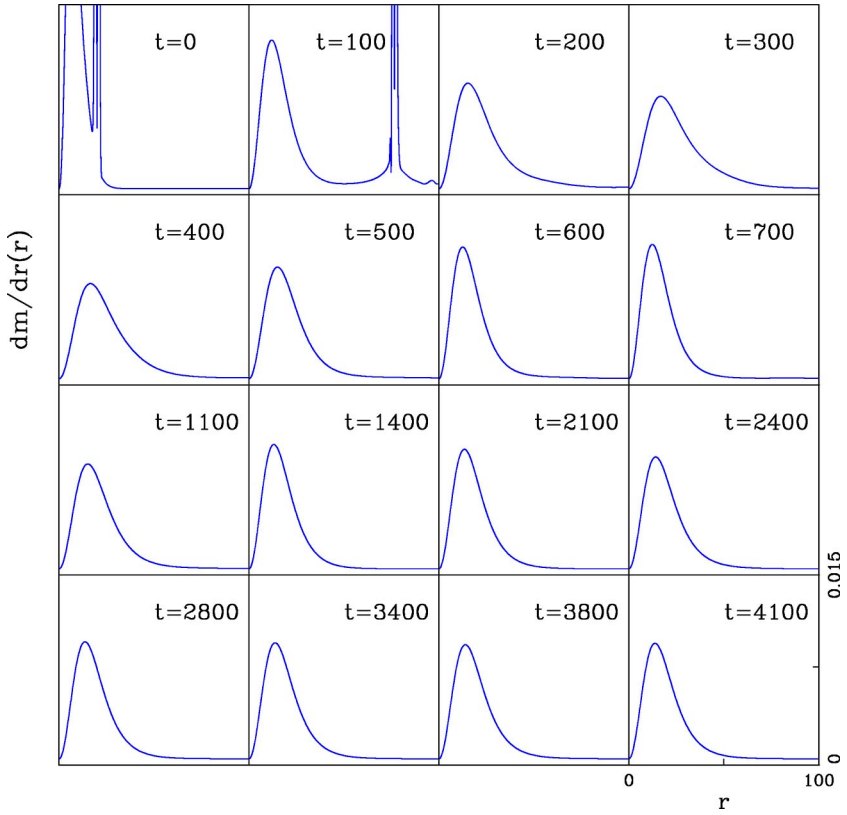

FIG. 2. This plot shows a sequence of snapshots of a typical ''sphaleron star'' evolution. The majority of the fields disperse within the first few frames after which the regular solution emerges and begins to settle down. Notice that times 700–1400, 2100–2800, and 3400–4100 show the maximum, median, and minimum values of three different oscillations. As can be seen, the first oscillation is quite pronounced, whereas by the third the amplitude of oscillation is negligible and we are approaching a static, stable solution. The solution would appear to be the same to within a few percent for any values of the initial data that do not produce a black hole. The mass of the final sphaleron star solution is $\approx(10-20)\%$ of the mass of the initial configuration. Note that in setting the scale of the vertical axis, the top portions of the fields in the first two frames have been cut off. This has been done to emphasize the damped oscillations in subsequent frames showing the stable solution. For this evolution, we used 10401 mesh points and a Courant factor of 0.5 along with $\eta=0.1$ and $\lambda=0.5$.

some of that gauge freedom by choosing $v\equiv 0$. This choice effectively eliminates the r dependence in the above gauge transformation. If we choose to work within the so-called ''magnetic ansatz'' we can fix the remaining freedom in the following way. It can be shown that in this ansatz, the component u is a function only of t, i.e., it is now pure gauge and can be set to zero as part of our gauge fixing. The remaining fields w and $\tilde{w}$ under the remaining constant gauge transformations are merely sent into linear combinations of each other and hence we can fix the last bit of gauge freedom by setting $w=0$. This leaves $\tilde{w}$ as the sole non-zero component of the gauge potential, the same form as in [9,10].[2] Our form for the Higgs field, taken from [9], is

$$\Phi=\frac{1}{\sqrt{2}}(\gamma\mathbf{1}-2\psi\tau_r)\begin{pmatrix}0\\1\end{pmatrix} \tag{10}$$

[2]If we had chosen not to work within the restriction of the magnetic ansatz, our gauge freedom would only have allowed us to set $v=0$ leaving us with three Yang-Mills functions which would need to be evolved [9,11].

and though not strictly spherically symmetric, results in a spherically symmetric energy density [6]. We will consider in this work only the case in which $\psi=0$. This is not a gauge choice but an additional assumption made merely to simplify the resulting equations and dynamics. A similar thing is done, for instance, in [9,10].

With these assumptions, the evolution equations for the Yang-Mills field become

$$\dot{\tilde{w}}=\frac{\alpha}{a}P+\beta Q \tag{11}$$

$$\dot{Q}=\left(\frac{\alpha}{a}P+\beta Q\right)' \tag{12}$$

$$\dot{P}=\left(\beta P+\frac{\alpha}{a}Q\right)'+\frac{\alpha a\tilde{w}}{r^2}(1-\tilde{w}^2)-\frac{\alpha a}{4}\gamma^2(\tilde{w}-1) \tag{13}$$

while the evolution equations for the Higgs field are given as

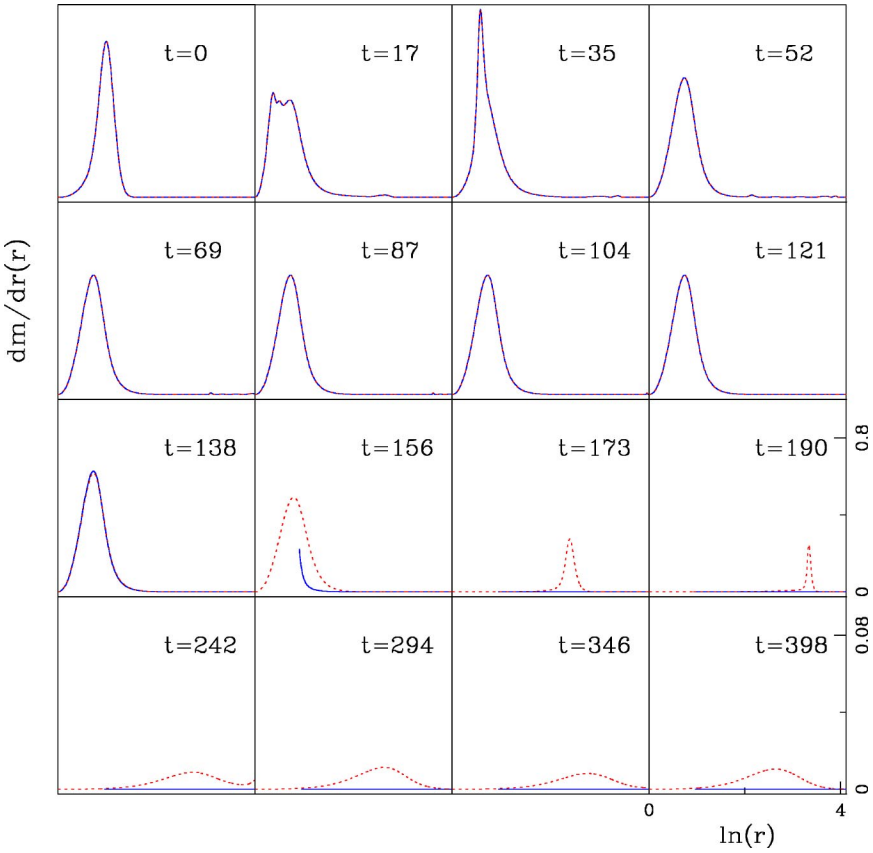

FIG. 3. This plot shows two near-critical solutions on the boundary between the Schwarszchild collapse and sphaleron star formation. The critical line between these two possibilities is characterized by the quasi-static regular solution visible between $t=52$ and $t=138$. This solution acts as an attractor for both near-critical evolutions. The final state is determined by the initial data values and is reflected in the evolution away from the attractor. In the one case (solid line), the majority of the configuration collapses to form a Schwarschild black hole with a mass gap consistent with type I transitions ($t=146$). In the regular, sphaleron case (dashed line), about (80–90)% of the mass disperses, leaving a stable, bound state with mass independent of the initial data and location along the critical line. The final, stable sphaleron star is fundamentally different from the quasi-static solution that acts as the attractor. Note that for visualization purposes, we have rescaled the vertical axis of the last four frames. In all frames, the horizontal axis remains unchanged and measures logarithmic radial coordinate. In addition, all fields are plotted so as to be exterior to any horizons. The gap present in the final seven frames for the evolution indicated by the solid line is intended to denote this together with the fact that the final solution on the black hole side (solid line) is Schwarzschild. For this evolution, we again used 10401 mesh points and a Courant factor of 0.5 along with $\eta=0.1$ and $\lambda=0.5$. The width of the Yang-Mills kink is $s=0.8$ and the binary search was over the center of the kink, x.

$$\dot{\gamma}=\frac{\alpha}{a}G+\beta E \tag{14}$$

$$\dot{E}=\left(\frac{\alpha}{a}G+\beta E\right)' \tag{15}$$

$$\dot{G}=\frac{1}{r^2}\left[r^2\left(\beta G+\frac{\alpha}{a}E\right)\right]'-\frac{\alpha a\gamma}{2r^2}(\tilde{w}-1)^2 - \frac{\lambda}{2}\alpha a\gamma(\gamma^2-2\eta^2), \tag{16}$$

$$\alpha''=\alpha'\left(\frac{a'}{a}-\frac{2}{r}\right)+\frac{2\alpha}{r^2}\left(a^2-1+\frac{2ra'}{a}\right)+4\pi G\alpha(S-3\rho) \tag{17}$$

$$a'=a\frac{1-a^2}{2r}+\frac{3}{8}ra^3K_r^{r2}+4\pi G\, ra^3\rho \tag{18}$$

$$K^{r\prime}{}_r=-\frac{3}{r}K^r{}_r+8\pi G\frac{1}{a}\left[\frac{PQ}{r^2}+\frac{1}{4}EG\right] \tag{19}$$

$$\beta=\alpha rK^{\theta}{}_{\theta}. \tag{20}$$

where, as usual, overdots, and primes denote differentiation with respect to t and r, respectively. Both of these sets of evolution equations are supplemented with the first order definitions $Q=\tilde{w}'$ and $E=\gamma'$ as well as the constraints on the metric components coming from the Einstein equations

The matter stress-energy terms in these equations are given by

$$\rho+S_r{}^r=\frac{P^2+Q^2}{a^2r^2}+\frac{E^2+G^2}{4a^2} \tag{21}$$

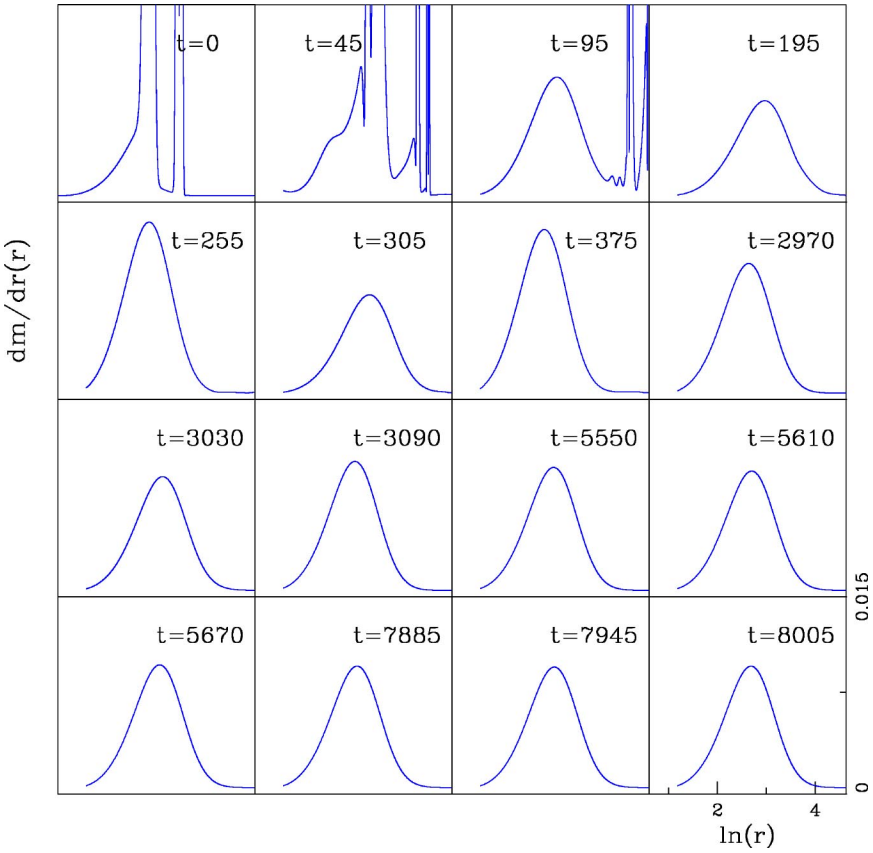

FIG. 4. This sequence of snapshots shows a typical evolution of a stable, hairy black hole solution at a generic point in the phase space. The first several frames show the partial dispersal of the initial fields and the formation of the black hole solution. In particular, times 2970–3090, 5550–5670, and 7885–8005 show the maximum, median, and minimum values of three oscillations. As can be seen the first oscillation is quite pronounced, while by the third, the solution is obviously settling down, ostensibly to a stable, hairy black hole. As in the previous figure, all fields are plotted so as to be exterior to any horizons. The gap in the solution in most of the frames for the evolution indicated by the solid line is intended to denote this. This run was done using 10400 points with a Courant factor of 0.5 and again with $\eta=0.1$ and $\lambda=0.5$.

$$\rho - S^r{}_r = \frac{(\tilde{w}^2-1)^2}{2r^4} + \frac{\gamma^2(\tilde{w}-1)^2}{8r^2} + \frac{\lambda}{16}(\gamma^2-2\eta^2)^2 \tag{22}$$

$$S^\theta{}_\theta = \frac{1}{8a^2}(G^2-E^2) + \frac{(\tilde{w}^2-1)^2}{4r^4} - \frac{\lambda}{32}(\gamma^2-2\eta^2)^2 \tag{23}$$

$$j_r = -\frac{PQ}{ar^2} - \frac{EG}{4a}. \tag{24}$$

Boundary conditions are implemented by demanding regularity at the origin and requiring the presence of only outgoing radiation at large distances (see [5]). The resulting constraints on the metric components require $\alpha'(t,0) = a'(t,0) = \beta(t,0) = K_r^r(t,0) = 0$. The matter fields may satisfy one of two possible regular configurations at the origin: either $\gamma(t,0)=0$ and $\tilde{w}(t,0)=-1$ or $\gamma'(t,0)=0$ and $\tilde{w}(t,0)=1$. These two choices correspond to the odd and even node solutions, respectively [9]. In order to find the critical solution we choose the former and look for the solution with a single unstable mode. The outgoing conditions require that at the edge of our grid,

$$P = -Q \tag{25}$$

$$\dot{Q} = \left[\left(\frac{\alpha}{a} - \beta\right)Q\right]' \tag{26}$$

$$G = \frac{1}{r}\left(\beta\frac{a}{\alpha} - 1\right)(\gamma - \sqrt{2}\eta) \tag{27}$$

$$\dot{E} = \left[\left(\beta - \frac{\alpha}{a}\right)\left(E + \frac{1}{r}[\gamma - \sqrt{2}\eta]\right)\right]'. \tag{28}$$

It should be noted that there is only one vacuum value for both the Yang-Mills and Higgs fields. That is to say at infinity, $\tilde{w}=1$ and $\gamma=\sqrt{2}\eta$. This can be contrasted with the model of [5] in which there are two vacuum states for the Yang-Mills potential in the absence of the Higgs field. For the initial pulse, we use a ''time-symmetric kink'' as in [5] for the gauge potential, namely,

$$w(0,r) = \left[1 + a\left(1 + \frac{br}{s}\right)e^{-2(r/s)^2}\right]\cdot\tanh\left(\frac{x-r}{s}\right) \tag{29}$$

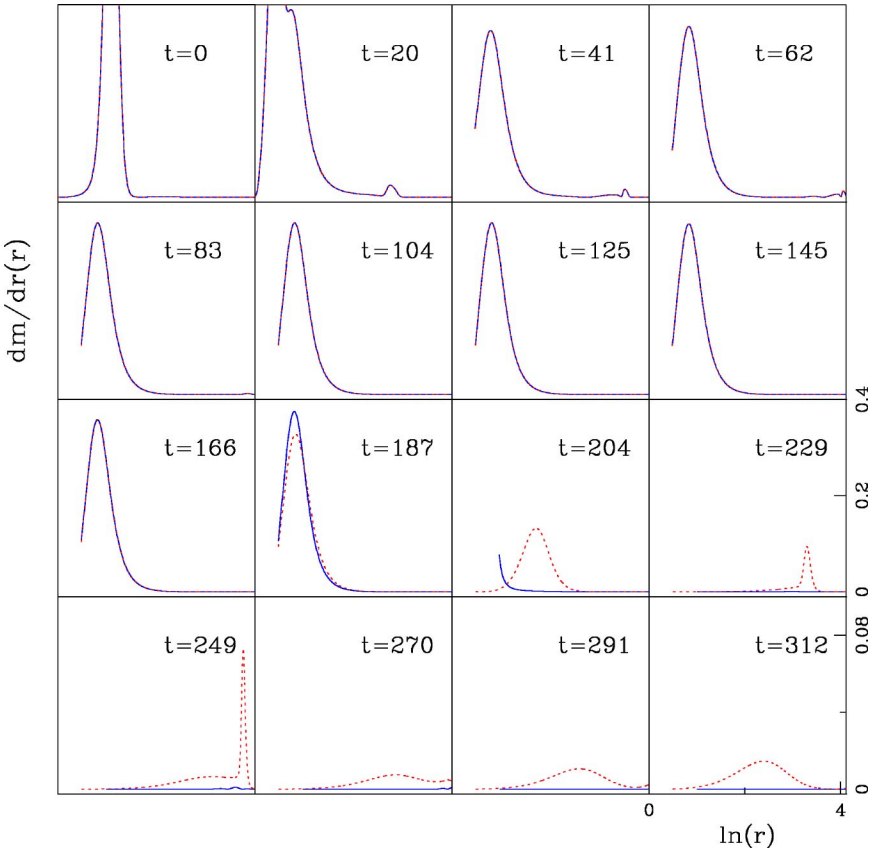

FIG. 5. This plot shows two near-critical evolutions on the border between the Schwarszchild and hairy black hole formation. The critical line between these two possibilities is characterized by a family of black holes parametrized by their horizon radius and possessing non-trivial Yang-Mills-Higgs hair outside the horizon. These colored black holes serve as the attractors for these two types of collapse and can be seen here between $t=41$ and $t=166$. The final state of the collapse can be distinguished by the subsequent evolution of the fields away from the attractor. On the Schwarzschild side (the solid line), the hair falls into the horizon (at $t\approx 204$), adding to the mass of the black hole, and resulting finally in a Schwarschild black hole. On the hairy side (the dashed line), the majority of the hair disperses to infinity. However, between 10 and 20% of the initial mass of the system (depending on where one is along the critical line) remains behind, eventually settling down and forming stable, Yang-Mills-Higgs hair outside a black hole. Note that the horizontal axis is the natural logarithm of the radial coordinate and that in the final four frames, the vertical axis is rescaled to visualize better the remaining hair in the hairy case. Again, all fields have been plotted so as to be exterior to any horizons. The gap(s) present in the plotted solutions is intended to denote this. This evolution used 10401 mesh points, a Courant factor of 0.5 and again had $\eta=0.1$ and $\lambda=0.5$. The width of the Yang-Mills kink is $s=0.7$ and the binary search was over the center of the kink, x.

$$\dot{w}(0,r)=0 \tag{30}$$

where the parameters a and b are chosen so that $w(0,0)=-1$ and $w'(0,0)=0$. The parameters x and s are the center and width of the kink, respectively.

The Higgs field is initialized as

$$\gamma(0,r)=\sqrt{2}\,\eta\tanh\frac{r}{\delta}+A_H\,e^{-(r-r_0)^2/d^2} \tag{31}$$

$$\dot{\gamma}(0,r)=0 \tag{32}$$

where the parameter δ is usually set to $\delta=10$. This is primarily due to the fact that varying δ does not significantly change the final result of the collapse. As a consequence, we perturb the Higgs field via a Gaussian pulse. Similar to the initialization for the Yang-Mills field, the parameters A_H, r_0, and d which describe the initialization of the Higgs field represent the amplitude, center, and width of the Gaussian pulse, respectively. These initial data parameters for the Yang-Mills and Higgs fields will constitute our initial dataset and will be used when tuning our evolutions to the critical solutions.

Our numerical approach closely follows that of [5]. We use a uniform grid recognizing that we will not have sufficient resolution to investigate type II collapse in a completely satisfactory way. Nonetheless, we have indications verifying the existence of type II behavior in our model. For this paper, therefore, we focus our primary interest on the black hole transition and the dynamics occurring within the black hole regime.

We use an iterative Crank-Nicholson scheme for the evolution equations while for the constraints, we simply integrate outward from the origin. As we want to consider evolutions that extend to the future of the black hole formation, our use of maximal slicing is crucial. In our coordinates, the apparent horizon equation is an algebraic relation

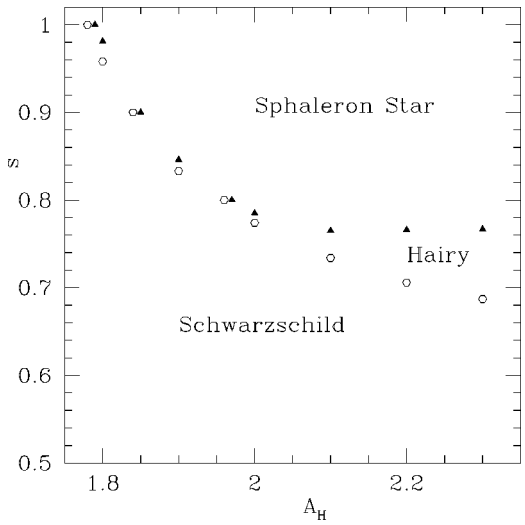

FIG. 6. This plot is of the initial data space and illustrates the end states of collapse as the width s and center x of the initial Yang-Mills field are varied. The Higgs field is in the ''pulse'' configuration, i.e., $r_0=20$, $d=1.05$, and $A_H=0.03$. The filled triangles represent the boundary between the formation of the sphaleron stars and the hairy black holes. The open hexagons depict the colored critical solutions on the boundary between the Schwarszchild and hairy black holes. Near these critical solutions, the type is depicted not only by the existence of the stable hair, but also by the transient hair either dispersing or falling down the horizon. Note the lack of filled hexagons, existent in Fig. 1, which would represent a type I transition from the sphaleron star to the black hole formation. Thus there is no triple point found in this slice of phase space. Each point depicted on the plot represents an evolution in which $|p-p^*|<10^{-5}$. For each evolution we again used 10401 mesh points and a Courant factor of 0.5 along with $\eta=0.1$ and $\lambda=0.5$.

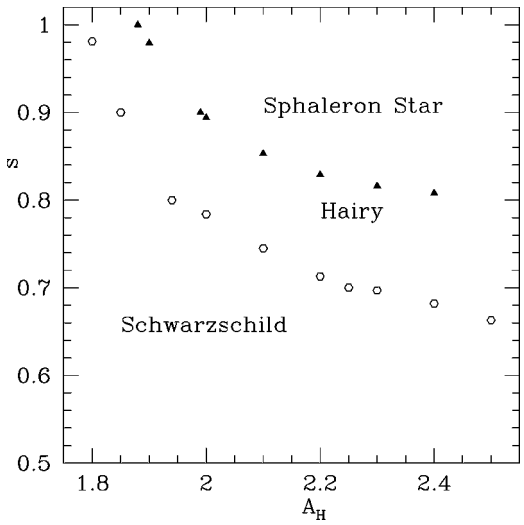

FIG. 7. This plot is of the initial data space and illustrates the end states of collapse as the width s and center x of the initial Yang-Mills field are varied. The Higgs field is in the ''pulse'' configuration, i.e., $r_0=20$, $d=1.05$, and $A_H=0.06$. The filled triangles represent the boundary between the formation of the sphaleron stars and the hairy black holes. The open hexagons depict the colored critical solutions on the boundary between the Schwarszchild and hairy black holes. Near these critical solutions, the type is depicted not only by the existence of the stable hair, but also by the transient hair either dispersing or falling down the horizon. Note the lack of filled hexagons, existent in Fig. 1, which would represent a type I transition from the sphaleron star to the black hole formation. Thus there is no triple point found in this slice of phase space. It is easy to see that the seperation of the sphaleron solution from the Schwarzschild black holes has increased from Fig. 6. Each point depicted on the plot represents an evolution in which $|p-p^*|<10^{-5}$. For each evolution we again used 10401 mesh points and a Courant factor of 0.5 along with $\eta=0.1$ and $\lambda=0.5$.

$$arK^{\theta}{}_{\theta}=1. \tag{33}$$

We use the same black hole excision technique developed in [12] and used in [5]. As discussed there, we set a threshold value slightly larger than 1 such that if $arK^{\theta}{}_{\theta}$ exceeds that value for certain grid points, we discard those points at future time steps considering them inside the apparent horizon. At the boundary of this region, we need no new boundary conditions for the evolution equations. For those variables solved via constraint equations we either switch to solving an evolution equation subsequent to the formation of a horizon or we ''freeze'' the variable (e.g. α) such that it retains the value it had when the horizon formed [5]. As a result, though we can observe matter falling into the horizon, we cannot comment on any dynamics within the apparent horizon as the evolution is effectively frozen for values of the radial coordinate less than the horizon radius. This procedure thus allows us to evolve past the formation of the black hole and thereby investigate such things as the final end states as well as the critical dynamics in the vicinity of transition regions.

We have tested the resulting code and shown it to be second-order convergent and to conserve mass. It also reproduces the results of [5] in the limit where the Higgs field and its coupling vanish. Finally, we note that we made extensive use of RNPL (rapid numerical prototyping language) [13], a language written expressly to aid the differencing and solution of partial differential equations.

III. RESULTS

In attempting to evolve these equations, it quickly became clear that the size of the initial data sets that could be varied is somewhat unwieldy and we had to make choices in order to restrict the possible sets of initial data parameters. Although we have performed numerous evolutions by varying the elements of different sets of initial data parameters, we will focus on the evolution of two sets of parameters to highlight our results. Other sets would appear to give qualitatively similar conclusions. When we evolve these equations, we confirm many of the same aspects that have come to be expected in similar models. However, there are, at the same time, a number of unexpected surprises.

To begin our examination of the dynamics of this model, we consider varying two parameters describing the initialization of the gauge potential, namely x and s, the center and width of the kink, respectively. The amplitude of the perturbing Gaussian pulse for the Higgs field is set to zero, $A_H=0$, and the width of the tanh function describing the Higgs field is $\delta=10$. We call this configuration the ''bland'' Higgs

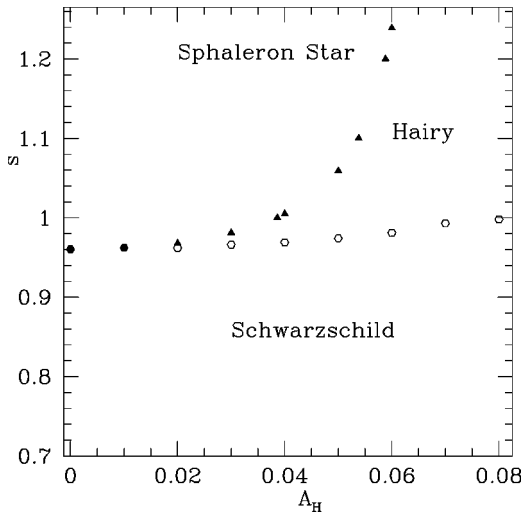

FIG. 8. This is another plot of the initial data space and illustrates the end states of collapse as the width s of the initial Yang-Mills field and the amplitude A_H of the Higgs pulse are varied, with $r_0=20$, $d=1.05$, and $x=1.8$. This plot intersects Fig. 1 at the line defined by $x=1.8$ and $A_H=0$. It should be noted that the structure for negative values of A_H is symmetric across the s axis. Again, the filled hexagons denote the boundary between the sphaleron stars and the Schwarzschild black holes, the filled triangles represent the boundary between the sphaleron stars and the hairy black holes while the open hexagons denote the location of the critical solutions separating the Schwarszchild and hairy black holes. In this mixed phase space, we find a small region in which we have a type I transition. As a result, it would appear that this portion of the initial data space contains a triple point. Note the difference in the limits of the vertical axis in this and Fig. 1. Each point on the respective critical lines represents a critical solution at a level $|p-p^*|/p^*<10^{-5}$. For each evolution we again used 10401 mesh points and a Courant factor of 0.5 along with $\eta=0.1$ and $\lambda=0.5$.

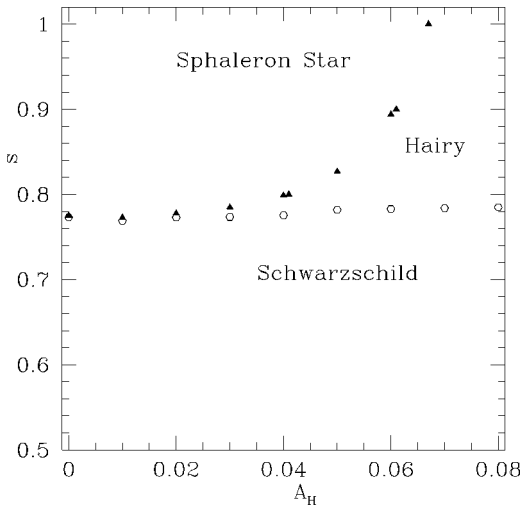

FIG. 9. This is another plot of the initial data space and illustrates the end states of collapse as the width s of the initial Yang-Mills field and the amplitude A_H of the Higgs pulse are varied, with $r_0=20$, $d=1.05$, and $x=2$. This plot intersects Fig. 1 at the line defined by $x=2$ and $A_H=0$. It should be noted that the structure for negative values of A_H is symmetric across the s axis. Again, the filled triangles represent the boundary between the sphaleron stars and the hairy black holes while the open hexagons denote the location of the critical solutions separating the Schwarszchild and hairy black holes. Note that the overlap of some of the polygons denotes only that the boundaries are near one another, not that they overlap. In this mixed phase space, we find no region with a type I transition. As a result, it would appear that this portion of the initial data space does not contain a triple point. Note the similarity in the limits of the vertical axis in this and Fig. 1. Each point on the respective critical lines represents a critical solution at a level $|p-p^*|/p^*<10^{-5}$. For each evolution we again used 10401 mesh points and a Courant factor of 0.5 along with $\eta=0.1$ and $\lambda=0.5$.

field. Note that in this section, all the pictured results are for values of the Higgs coupling parameters, $\eta=0.1$ and $\lambda=0.5$. A region of this slice of the phase space is shown in Fig. 1.

On varying the center and width of the Yang-Mills potential, $\tilde{w}$, one finds three distinct regions of the initial data space. These correspond, as in [5], to two distinct black hole regions, and a ''dispersive'' region in which no black hole forms. On the boundaries between these regions sit appropriate critical solutions. It is worth noting, however, that in the region in which no black hole forms, we no longer observe the complete dispersal of all the matter fields. Instead, while a majority of the fields do escape to infinity, a nontrivial portion of the fields forms a bound state, or ''sphaleron star.'' Shortly after formation, this solution oscillates rapidly, but settles down to what appears to be a static solution. Long evolutions with $t\sim 30000M$ (with M the initial mass of the spacetime) confirm the stability of this solution. The mass of this stable star is, to within a few percent, independent of any of the initial field parameters. The solution and its mass do appear to depend on the coupling parameters η and λ [6]. Snapshots of a typical evolution in the dispersive regime are shown in Fig. 2.

In one of the black hole regions, we note no significant change in the dynamics from those similarly exhibited in [5]. The collapsing matter forms a black hole with finite mass which, after the residual fields have dispersed to infinity, settles down to the Schwarzschild solution. On the type I critical line separating the black hole formation and the sphaleron star configuration, we find a regular sphaleron as the critical solution analogous to the Bartnik-McKinnon $n=1$ solution. An example of the critical behavior at this type I transition is given in Fig. 3 in which a sub-critical and a super-critical evolution are shown.

Within the other black hole region, however, there are some new features. As in [5], this region is again characterized by the dynamical formation of a black hole with finite mass. As the critical line which separates dispersion (or strictly, the sphaleron star formation) from the black hole region is approached, the mass of these black holes begins to decrease such that we interpret the critical transition as type II. However, the black holes that form away from the critical line after the transient hair has dispersed to infinity do not settle down to the Schwarzschild black holes. Instead, the final end state would appear to be a stable, colored black hole with non-trivial Yang-Mills and Higgs fields outside the event horizon. This, of course, is analogous to the sphaleron star that forms in the no-black-hole region of this system

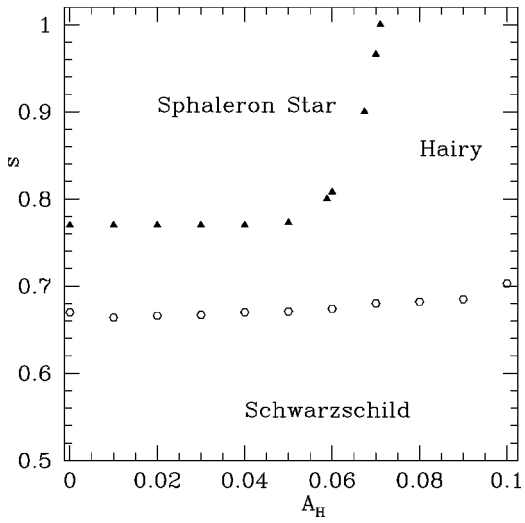

FIG. 10. This is another plot of the initial data space and illustrates the end states of collapse as the width s of the initial Yang-Mills field and the amplitude A_H of the Higgs pulse are varied, with $r_0=20$, $d=1.05$, and $x=2.4$. This plot intersects Fig. 1 at the line defined by $x=2.4$ and $A_H=0$. It should be noted that the structure for negative values of A_H is symmetric across the s axis. Again, the filled triangles represent the boundary between the sphaleron stars and the hairy black holes while the open hexagons denote the location of the critical solutions separating the Schwarszchild and hairy black holes. In this mixed phase space, we find no region with a type I transition. As a result, it would appear that this portion of the initial data space does not contain a triple point. Note the similarity in the limits of the vertical axis in this and Fig. 1. Also note the increased seperation between the sphaleron solutions and the Schwarzschild black holes, compared to the previous two figures. Each point on the respective critical lines represents a critical solution at a level $|p-p^*|/p^*<10^{-5}$. For each evolution we again used 10401 mesh points and a Courant factor of 0.5 along with $\eta=0.1$ and $\lambda=0.5$.

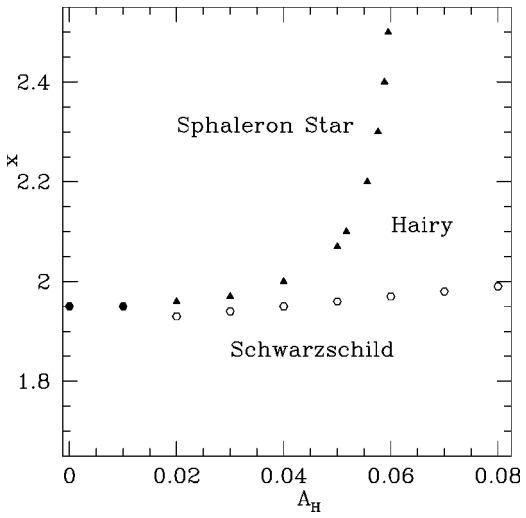

FIG. 11. This is another plot of the initial data space and illustrates the end states of collapse as the center x of the initial Yang-Mills field and the amplitude A_H of the Higgs pulse are varied, with $r_0=20$, $d=1.05$, and $s=0.8$. This plot intersects Fig. 1 at the line defined by $s=0.8$ and $A_H=0$. It should be noted that the structure for negative values of A_H is symmetric across the x axis. Again, the filled hexagons represent the boundary between the sphaleron stars and the Schwarzschild black holes with type I transitions, the filled triangles represent the boundary between the sphaleron stars and the hairy black holes while the open hexagons denote the location of the critical solutions separating the Schwarszchild and hairy black holes. In this mixed phase space, we find a small region in which type I behavior borders the region of the sphaleron star formation. As a result, it would appear that this portion of the initial data space contains a triple point. Each point on the respective critical lines represents a critical solution at a level $|p-p^*|/p^*<10^{-5}$. For each evolution we again used 10401 mesh points and a Courant factor of 0.5 along with $\eta=0.1$ and $\lambda=0.5$.

rather than the complete dispersal of the fields seen in [5]. The basic dynamics in this case are illustrated in Fig. 4. The collapsing configuration forms a finite mass black hole with a significant portion of the remaining field escaping to infinity. Nevertheless, some of the hair remains behind and within the vicinity of the event horizon. This hair oscillates for some time and eventually settles down to a stable configuration. Evolutions of the order of $t\sim 30000M$ show no appreciable diminution or instability in the fields.

The mass of the hair in these black hole solutions also seems to be independent of the initial data parameters. Though the radius of the black hole will vary with the initial parameters, the exterior mass remains unchanged. This observation is consistent with and similar to that for the sphaleron stars in which a single stable, regular solution is found throughout the no-black-hole region. In addition, like their regular counterparts, the black hole solutions will depend on the parameters η and λ. Curiously, the mass of this exterior hair is very nearly the same value as the mass of the sphaleron star. Thus, in one sense, these hairy black hole solutions can be thought of as sphaleron star solutions within which the central density increases to the point where a horizon forms. This is similar in turn to gravitating 't Hooft–Polyakov monopoles. For certain values of the coupling, the monopoles can have a black hole form at their center.

For the solutions near the threshold separating the black hole formation and dispersion, we find hints that these are indeed type II critical solutions and that the black hole mass scales as expected. However, we stress again that our unigrid code is not able to settle this issue definitively and that it awaits additional study.

We are able, though, to consider the transition between the different types of dynamical collapse in the black hole regime. Again, we find a family of critical solutions separating the Schwarszchild and hairy black holes. These critical solutions are themselves sphaleron black holes parametrized by their horizon radius such that as one moves away from the ''triple point'' in Fig. 1, the radius increases. On the hairy side of this line, near-critical evolutions have dynamics described above with the collapsing configuration forming a black hole of finite mass with non-trivial hair outside. However, as the transition between the hairy and Schwarszchild black holes is approached, there is an intermediate solution—a hairy black hole—which forms and to which the evolving solution is attracted. This intermediate solution is unstable and eventually collapses. For initial configurations on the hairy side, the collapse is distinctive in that very little

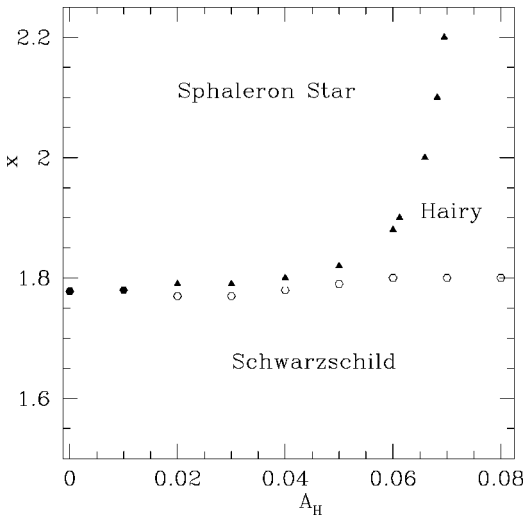

FIG. 12. This is another plot of the initial data space and illustrates the end states of collapse as the center x of the initial Yang-Mills field and the amplitude A_H of the Higgs pulse are varied, with $r_0=20$, $d=1.05$, and $s=1.0$. This plot intersects Fig. 1 at the line defined by $s=1.0$ and $A_H=0$. It should be noted that the structure for negative values of A_H is symmetric across the x axis. Again, the filled hexagons represent the boundary between the sphaleron stars and the Schwarzschild black holes with type I transitions, the filled triangles represent the boundary between the sphaleron stars and the hairy black holes while the open hexagons denote the location of the critical solutions separating the Schwarszchild and hairy black holes. In this mixed phase space, we find a small region in which type I behavior borders the region of the sphaleron star formation. As a result, it would appear that this portion of the initial data space contains a triple point. Each point on the respective critical lines represents a critical solution at a level $|p-p^*|/p^*<10^{-5}$. For each evolution we again used 10401 mesh points and a Courant factor of 0.5 along with $\eta=0.1$ and $\lambda=0.5$.

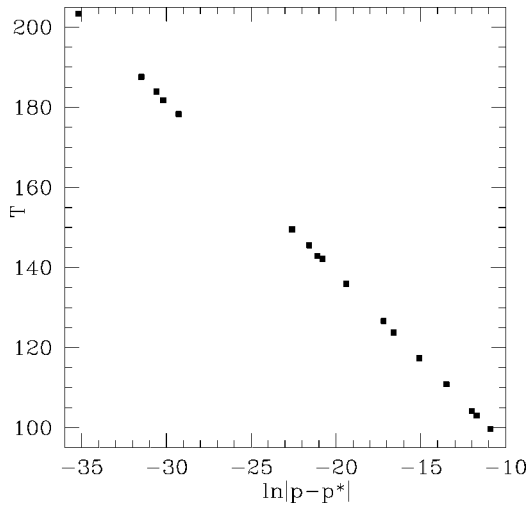

FIG. 13. This plot gives the elapsed time (as measured by an observer at infinity) spent by an evolving configuration in the sphaleron regime as the critical line separating the Schwarszchild black holes and the sphaleron star formation is approached. On the black hole side of the critical solution, there is a scaling relation for the time given by $T=-\lambda_1|p-p^*|$ where λ_1 is the inverse Lyapunov exponent of the corresponding unstable mode of the critical solution sitting on the threshold between the black hole formation and sphaleron star formation. In the current case, we find from a least squares fit that $\lambda_1=4.27(1)$. We define the elapsed time T as the time from the beginning of the evolution until the pulse crosses $r=40$. As before, for these evolutions, we used 10401 mesh points and a Courant factor of 0.5 along with $\eta=0.1$ and $\lambda=0.5$.

of the exterior fields falls into the black hole. Rather, some of it is dispersed to infinity while the remainder reconstitutes in a new and different colored configuration outside the black hole already present. This is shown in Fig. 4 for a generic collapse in the hairy regime as well as in the last frames of Fig. 5 for a near-critical evolution.

On the Schwarszchild side of the critical line, similar near-critical evolutions exhibit the same early time dynamics with the formation of a finite mass black hole and the approach to the intermediate hairy black hole. However, as the critical line is approached, this unstable black hole now collapses and loses most of its hair into the black hole causing it to grow in size. A picture of both collapse dynamics is shown in Fig. 5.

If we allow the amplitude of the Higgs field to be nonzero, i.e., explore the ''pulse'' Higgs configuration, we see that a slightly different phase space structure exists. The sphaleron star region of the space is completely bounded by a type II critical transition. The Schwarschild black holes no longer make a critical transition into the sphaleron stars. Instead, the hairy black holes exist in a thin shell dividing the Schwarschild and sphaleron solutions. Thus, in these slices of phase space, the triple point is not present. This is shown in Figs. 6 and 7 for amplitudes of 0.03 and 0.06, respectively.

So far, our entire description has been within the context of varying two of the initial data parameters that describe the Yang-Mills field, while keeping the values of the Higgs parameters fixed. The natural thing to do is to extend our search into phase space regions in which we vary one Yang-Mills parameter and one Higgs parameter. We choose to vary the amplitude of the Higgs field along with the Yang-Mills parameters. It should be noted that we could choose to vary the center or width of the Higgs pulse. But, in order to minimize the size of the phase space under investigation, we explore regions where the width and center are fixed at the values 20 and 1.05, respectively. These regions of the phase space are shown in Figs. 8–12. Note the existence of the triple point in some regions, and its absence in others. This suggests that, in our three dimensional phase space, this triple ''point'' is not a true point, but is a line of finite extent.

Finally, we note that the critical solutions separating the Schwarszchild black hole formation from the sphaleron star formation and the two types of collapse exhibit time scaling as would be expected. As the single, unstable mode characteristic of each critical solution is tuned out, near-critical solutions spend increasing amounts of time as measured by an asymptotic observer on the critical solution. These scaling relations are given by $T\approx-\lambda\ln|p-p^*|$ where λ is the characteristic time scale for the collapse of the unstable critical solution. It corresponds to the inverse Lyapunov exponent of the unstable mode. Such scaling relations specific to points on the relevant critical lines are shown in Figs. 13 and 14.

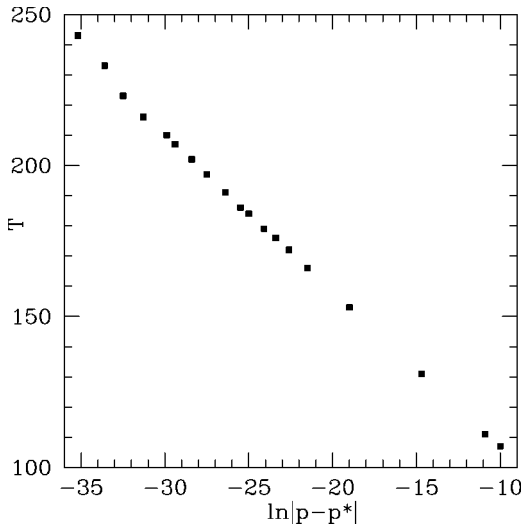

FIG. 14. This graph gives the elapsed time (as measured by an observer at infinity) spent by an evolving configuration in the hairy black hole region as the critical line separating the Schwarszchild and hairy black holes is approached. As the critical solution is approached, the evolution spends more and more time on the critical solution and we expect a linear relationship between that time and logarithmic distance in the initial data space: $T=-\lambda_{\mathrm{I-II}}|p-p^*|$. The slope of this line, $\lambda_{\mathrm{I-II}}$, is the inverse Lyapunov exponent of the corresponding unstable mode of the critical solution. From a least squares fit, we find $\lambda=5.27(1)$. The time on the critical solution is defined as the time between the beginning of the evolution until the pulse in the type II case crosses $r=40$. As before, for these evolutions, we used 10401 mesh points and a Courant factor of 0.5 along with $\eta=0.1$ and $\lambda=0.5$.

IV. DISCUSSION

We have presented evidence for critical phenomena in the gravitational collapse of $SU(2)$ sphaleron configurations of the Yang-Mills-Higgs fields. In many respects, this collapse is qualitatively similar to that in the Einstein-Yang-Mills system but does have some notable suprises. The critical behavior is seen again in three possible transitions. On each of these transitions sit critical solutions which serve as intermediate attractors for nearby evolutions in the initial data space. Near the critical line separating the Schwarszchild black holes from the regular solution as well as for the critical line separating the two types of dynamical black hole formation, there are time scaling relations as the near-critical solutions approach the critical solutions. In addition, the mass of the black holes formed in the appropriate region will exhibit a mass gap in crossing these critical lines. Near the critical line separating the hairy black holes from the regular end state region, we have indications that the mass of the black hole scales without a mass gap, but again, due to our unigrid code, we cannot settle this conclusively although expectations and indications would bear this out.

Among the surprises in this model are that in certain regions of the initial data space, we find that regular, stable, sphaleron solutions are produced rather than the purely dispersive regime seen in [5]. However, we also have stable, hairy black holes produced in the supercritical, black hole regime. This contrasts again with earlier results in which the end state in spherical symmetry was always a Schwarzschild black hole. Within one region, the end state is always a Schwarzschild black hole with the exterior gauge and Higgs fields either falling into the existing black hole or dispersing to infinity. In the other region, the final black holes are stable, hairy black holes. It is worth reemphasizing that the colored black hole solutions sitting on the critical line separating the types of black hole collapse are not the same as the stable, colored black holes that are the final end states in one of the supercritical regions. This can be seen most easily in Fig. 5.

It is also noteworthy that the existence of all the solutions which we find is contingent on the magnetic ansatz within which we have chosen to work. In general, both the regular and colored black hole solutions which we find to be the stable end states of collapse are expected to be unstable based on a linear perturbation analysis [10]. However, such an analysis assumes that both the gravitational and sphaleron sectors in the theory are perturbed. Our evolutions perturb only the gravitational sector. It is reasonable to assume that the stable solutions which we find will become unstable on perturbation of the Yang-Mills gauge field away from the magnetic ansatz. We hope to address this issue in future work.

Another noteworthy issue is the structure of the initial data space. A curiosity of our current results is that the triple point is not present in every two-dimensional slice of the phase space, but seems to be present within some finite interval. As a result, in some regions of the phase space the boundary between the regular end states (the sphaleron star formation here) and the black hole formation is taken up entirely by a type II transition.

Nonetheless, given the structure of the initial data space, one can draw an analogy with the gravitating monopole case in which a small black hole can form within a 't Hooft–Polyakov monopole coupled to gravity. This stable object can be rendered unstable above a maximum value of the horizon radius at which point the exterior Yang-Mills-Higgs hair will either fall into the black hole or disperse leaving a final Schwarzschild black hole. A similar thing happens in the current sphaleron case. For example, following a line of constant x in Fig. 1 that intersects each region, we see that as s decreases, one can interpret the process in a similar way. A regular solution develops a small, stable black hole at the center which (with decreasing width of the initial Yang-Mills potential, s) increases in size until the combined sphaleron and black hole system becomes unstable and is replaced with a larger Schwarzschild black hole. As a result, it would be interesting to consider the full dynamical evolution of the gravitating monopole and compare with the sphaleron case reported here.

ACKNOWLEDGMENTS

This research has been supported in part by NSF grants PHY-9900644 and PHY-0139782. E.W.H. would like to thank A. Wang for useful discussions as well as M. Choptuik and R. Marsa for their work on an earlier code which served as the precursor to the one described here.

[1] M.W. Choptuik, Phys. Rev. Lett. **70**, 9 (1993).
[2] C. Gundlach, Living Rev. Relativ. **2**, 4 (1999).
[3] G. Lavrelashvili and D. Maison, Phys. Lett. B **349**, 438 (1995); M.S. Volkov, O. Brodbeck, G. Lavrelashvili, and N. Straumann, *ibid.* **349**, 438 (1995).
[4] M.W. Choptuik, T. Chmaj, and P. Bizon, Phys. Rev. Lett. **77**, 424 (1996).
[5] M.W. Choptuik, E.W. Hirschmann, and R.L. Marsa, Phys. Rev. D **60**, 124011 (1999).
[6] D. Maison, ''Solitons of the Einstein-Yang-Mills theory,'' gr-qc/9605053.
[7] R.F. Dashen, B. Hasslacher, and A. Neveu, Phys. Rev. D **10**, 4138 (1974).
[8] E. Witten, Phys. Rev. Lett. **38**, 121 (1977).
[9] B.R. Greene, S.D. Mathur, and C.M. O'Neill, Phys. Rev. D **47**, 2242 (1993).
[10] P. Boschung, O. Brodbeck, F. Moser, N. Straumann, and M. Volkov, Phys. Rev. D **50**, 3842 (1994).
[11] M.S. Volkov and D.V. Gal'tsov, Phys. Rep. **319**, 1 (1999).
[12] R.L. Marsa and M.W. Choptuik, Phys. Rev. D **54**, 4929 (1996).
[13] R.L. Marsa and M.W. Choptuik, ''The RNPL User's Guide.'' http://laplace.physics.ubc.ca/People/marsa/rnpl/users_guide/users_guide.html (1995); Software available from http://laplace.physics.ubc.ca/Members/matt/Rnpl/index.html